

Manipulability-based configuration evaluation of cooperative payload transport by mobile manipulator collectives

Chin Pei Tang and Venkat N. Krovi*

Department of Mechanical and Aerospace Engineering, State University of New York at Buffalo, Buffalo, NY 14260, USA
E-mail: chintang@eng.buffalo.edu

(Received in Final Form: May 8, 2006, First published online: August 24, 2006)

SUMMARY

In this paper, we focus on the development of a quantitative performance analysis framework for a cooperative system of multiple wheeled mobile manipulators physically transporting a common payload. Each mobile manipulator module consists of a differentially driven wheeled mobile robot (WMR) with a mounted planar three-degree-of-freedom (DOF) revolute-jointed manipulator. A composite cooperative system is formed when a payload is placed at the end-effectors of many such modules. The system possesses the ability to change its relative configuration as well as to accommodate relative positioning errors of the wheeled agents. However, the combination of nonholonomic constraints due to the mobile bases, holonomic constraints due to the closed kinematic loops, and the different joint-actuation schema (active/passive/locked) within the system requires careful quantitative evaluation to efficiently realize the payload manipulation task. Hence, in this paper, we extend the differential kinematic model for treatment of constrained articulated mechanical systems to formulate a framework to include both the mixture effect of holonomic/nonholonomic constraints and the different possible joint-actuation schema in our system. The system-level performance is then examined quantitatively by the manipulability measure in terms of isotropy index with representative case studies.

KEYWORDS: Cooperative robots; Mobile manipulator; Nonholonomic constraints; Closed-loop chains; Manipulability.

1. Introduction

Our overall goal is the design, analysis, and implementation of a modular, flexible, and scalable system of multiple wheeled mobile agents that are individually autonomous but can team up to cooperatively transport large payloads. Such frameworks for remotely controlled or remotely supervised cooperation of multiple autonomous mobile robots have applications for material-handling tasks in many fields.^{1,2}

In our design, the individual autonomous agents take the form of differentially driven wheeled mobile manipulators, consisting of an articulated arm attached to a mobile base. Each mobile base possesses a single rigid axle between two fixed disk wheels and the usual complement of nonholonomic

kinematic constraints. The attached articulated arm permits relative planar motion of the end-effector with respect to the mobile base in the horizontal plane. Various types of articulated arms³ have been examined for suitability for the proposed cooperative payload transport task. However, for this paper, we assume that the articulated arm has *three* revolute joints—forming the so-called Type III mobile manipulator shown in Fig. 1(a).

A composite multi-degree-of-freedom (MDOF) vehicle system is formed when a common payload is placed at the end-effectors of the two or more adjacent modules, as shown in Fig. 1(b). The attached arms act like a compliant suspension system, which with suitable instrumentation and actuation endows the composite system with (a) ability to accommodate changes in the relative configuration; (b) redundant sensing for localizing the modules; and (c) redundant actuation for moving the common payload while compensating for environmental disturbances and errors.

In particular, these articulations (with at least three DOF) permit the relaxation of the requirement for a common *center of rotation* between the multiple axles created by the *nonholonomic constraints* at the wheels. However, while the velocity-level kinematic constraints for the system are eliminated, other holonomic constraints (due to the closed kinematic loops) are introduced between the relative motions of the bases. Such *closed kinematic loops* present a number of subtleties that are not often seen in open kinematic chain manipulators. Notably, the kinematic configuration space of a closed-loop manipulator is no longer a flat space but becomes a curved manifold embedded in a higher dimensional vector space. Further, as has been mainly discussed in this paper, the existence of such holonomic constraints limit the DOF of the systems, and hence not all articulations need to be actuated. Thus, the selection of the *location of the active/passive/locked joints* also plays a vital role in determining the overall performance of the system.

In this paper, we analyze the cooperative composite system within a constrained articulated mechanical system framework. Specifically, we focus on the kinematic modeling while taking into account (a) the nonholonomic constraints due to the wheel assemblies together with the holonomic constraints due to the kinematic closed loops and (b) the varying location and actuation of the joints within the system. Performance of several cooperative system scenarios with varying actuation arrangements are then quantified in terms of the system-level manipulability measure.

* Corresponding author. E-mail: vkrovi@eng.buffalo.edu

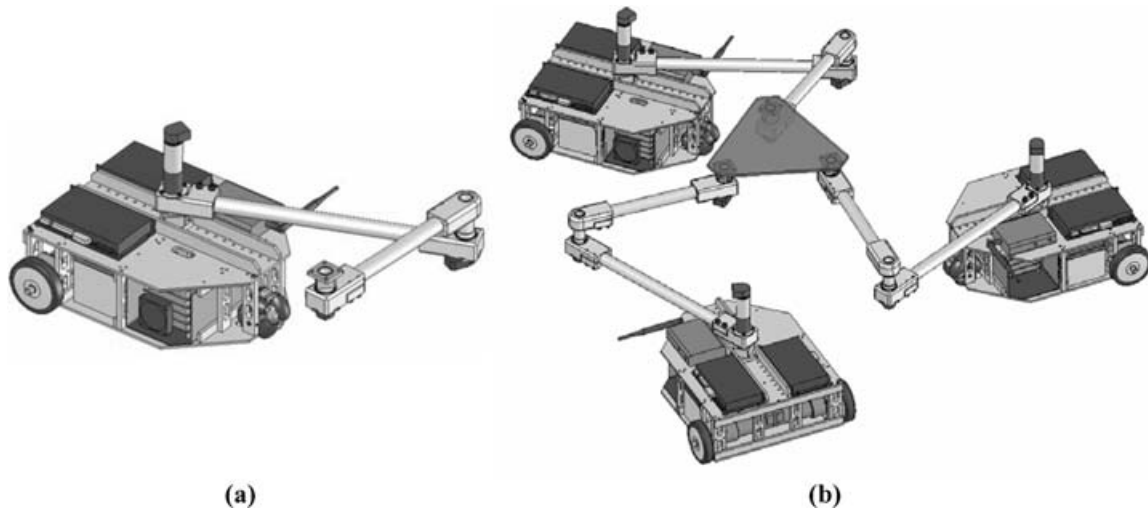


Fig. 1. (a) Representative mobile manipulator module. (b) Representative composite formation of cooperative system.

The rest of the paper is organized as follows: Section 2 presents a brief overview of the pertinent literature followed by the twist-based kinematic model of the wheeled mobile manipulator module presented in Section 3. This is then used in Section 4 to model the composite system with kinematic closed-loop constraints and formulate system-level manipulability-based measures-of-performance. Different case studies of cooperative payload transport with varying actuation schema are examined in Section 5 in terms of the manipulability measure. Finally, a brief discussion and concluding remarks are presented in Section 6.

2. Literature Survey

Cooperative multirobot systems, ranging from multiple mobile robots,^{4,5} multiple manipulators,⁶ multifingered hands,^{7,8} and multilegged vehicles^{9,10} have been extensively studied in a variety of contexts. In what follows, we restrict our attention to cooperative physical manipulation by articulated mechanical systems focusing solely on the motion distribution issues.

2.1. Cooperating articulated mechanical systems

The characteristic feature of such systems is the formation of closed kinematic chains, typically with one reference member interacting with a number of supporting serial chains. The nature of the attachment of the supporting chains to the reference member permits a *structural classification*¹¹ into *Type 0* systems (such as multiarm systems and dextrous hands), and *Type 1* systems (such as legged machines). At the same time, the presence of these closed kinematic chains reduces the effective DOF of the system, creating kinematic redundancy and most often redundancy in actuation.⁹ This permits an alternate *functional classification* into *underactuated*, *exactly-actuated*, and *redundantly actuated systems*.

2.2. Cooperating system of mobile manipulators

There is relatively less literature, but considerably greater variability, in the approaches employed for cooperation of

multiple mobile manipulators.^{12–16} Khatib *et al.*¹² developed a decentralized control structure for cooperative tasks with mobile manipulation systems with *holonomic bases* and *fully actuated* manipulators. Motion planning has also been considered for collaborating teams of nonholonomic mobile manipulators from various centralized perspectives.^{14,17} Kosuge *et al.*¹⁵ proposed a simple method for carrying a large object by cooperation of multiple mobile manipulators with *impedance-based controllers* by *selectively locking* and *unlocking* some joints of the mounted manipulators on mobile platforms. Yamakita *et al.*¹⁶ implemented the passive velocity field control approach for the cooperative control of multiple mobile robots holding an object. However, in most cases, the focus is on a fully actuated manipulator, without the possibility of including any passive or semipassive joints, which is a significant feature in our system.

The composite system formed by connecting the multiple mobile manipulators to the common payload also forms a subclass of the larger class of MDOF wheeled vehicles.^{18–24} While some of these like the RollerRacer¹⁸ and the Snakeboard¹⁹ are case studies in underactuated locomotion, several others like OMNIMATE/CLAPPER²⁰ and systems with multiple actively steered wheels^{21–23} and WAAVs²⁴ feature redundancy in actuation. Several of these authors also noted that despite gains in maneuverability over conventional mobile robots, the overconstrained nature with hybrid series-parallel kinematic chains creates challenges in planning and control of such wheeled systems.

Finally, immense variability in the overall composite system can arise due to the selection of the type of mobile base, the manipulator arm, and the number of such branches/legs attaching to the platform. For instance, Ben-Horin *et al.*²⁵ examined a system with three branches, each of which consisted of a spatial six-DOF manipulator mounted on omnidirectional bases (or as extended by Shoval and Shoham^{26,27} to wheeled bases translating along parallel straight lines). Our framework is intended to allow a far more general and systematic kinematic performance evaluation of a multimodule composite system—regardless of the number of modules, the type of mobile base, or the articulated structure of the mounted manipulator.

2.3. Performance measures

Performance measures play a critical role in the design, evaluation, optimization, and control of robotic systems. Performance measures for an individual robotic system are very well developed, including several Jacobian-based performance measures (JBPM), such as manipulability, singularity, and dexterity.²⁸ However, literature on the extension of such performance measures to groups of robots is relatively limited. Traditionally, variances in robots within a team were classified only as heterogeneous or homogeneous. Balch²⁹ developed a quantity called the social entropy to provide a quantitative evaluation of diversity and information-level cooperation in robot teams. Alternatively, energy-based measures,^{30,31} developed from left-invariant Riemannian metrics,³² have been used to characterize the total kinetic energy of a collective at any instant of time, or over the entire maneuver.

While these measures show considerable promise, in this paper, we focus our attention solely on Jacobian-based manipulability measures to serve as measure of motion and force transmission capability. Building from Yoshikawa's measure of manipulability³³ for the serial-chain case, a large variety of manipulability-based formulations have been used in different applications.^{8,34,35} The use of singular value decomposition (SVD) of the Jacobian matrix offers further mathematical and geometrical insight of the manipulability characteristics of a robotic system.²⁸ Efforts for characterizing the manipulability of parallel-chain mechanisms^{36–38} have noted the engendered difficulties. Such systems possess multiple closed kinematic loops whose loop closure constraints are responsible for considerable kinematic (and often actuation) redundancy within the system. Further, even in nonredundant settings, selection of the location of active/passive joints can significantly affect the manipulability, which is further explored in this paper. We adapt some aspects of the existing work,^{36–38} extending it to include nonholonomic constraints within the formulation to facilitate performance evaluation of our composite system.

3. Modeling of the Individual Modules

3.1. Mathematical preliminaries

We briefly summarize the necessary mathematical preliminaries and fix the notation used in our formulation. The reader is referred to refs. 3, 39 for further details.

In a two-dimensional Euclidean task space, the configuration of a rigid body can be represented as an element of $A \in SE(2)$. In our notation, the relative configuration of a body-fixed frame $\{E\}$ relative to an inertial-fixed frame $\{F\}$ can be defined by a 3×3 homogeneous transformation matrix of

$${}^F A_E = \begin{bmatrix} {}^F R_E & {}^F \underline{d} \\ \underline{0}^T & 1 \end{bmatrix} \quad (1)$$

where ${}^F R_E \in SO(2)$ is a rotation matrix, and ${}^F \underline{d} \in \mathbb{R}^2$ is a displacement vector. In planar case, a twist matrix $T \in se(2)$

can be represented by a 3×3 matrix in the form of

$$T = \begin{bmatrix} \Omega & \underline{v} \\ \underline{0}^T & 0 \end{bmatrix} \quad (2)$$

where $\Omega = \begin{bmatrix} 0 & -\omega \\ \omega & 0 \end{bmatrix} \in so(2)$ is a skew-symmetric matrix, $\omega \in \mathbb{R}$, and $\underline{v} \in \mathbb{R}^2$. A twist vector can then take the form of $\underline{t} = \begin{bmatrix} \omega \\ \underline{v} \end{bmatrix} \in \mathbb{R}^3$. Note that ω is an angular velocity scalar and \underline{v} is a linear velocity vector in the plane. In our context, a body-fixed twist matrix corresponding to the motion of body-fixed frame $\{E\}$ with respect to its *immediately preceding frame* $\{F\}$ (but as expressed in frame $\{E\}$) can be determined as

$${}^E [{}^F T_E] = [{}^F A_E^{-1}] [{}^F \dot{A}_E]. \quad (3)$$

Such a motion description is particularly useful in the study of locomotion systems, since it is invariant to the changes of the inertial-fixed frame. The resulting twist matrix can be transformed to any arbitrary frame $\{N\}$ by a similarity transformation as

$${}^N [{}^F T_E] = [{}^N A_E] {}^E [{}^F T_E] [{}^N A_E^{-1}]. \quad (4)$$

Finally, for an n -DOF serial chain, the end-effector twist can be expressed as a sum of twist contributions of the individual joints as

$$\begin{aligned} {}^n [{}^0 \underline{t}_n] &= {}^n [{}^0 \underline{t}_1] \dot{\theta}_1 + {}^n [{}^1 \underline{t}_2] \dot{\theta}_2 + \cdots \\ &\quad + {}^n [{}^{n-2} \underline{t}_{n-1}] \dot{\theta}_{n-1} + {}^n [{}^{n-1} \underline{t}_n] \dot{\theta}_n \end{aligned} \quad (5)$$

where each vector ${}^n [{}^{n-1} \underline{t}_n]$ represents the instantaneous screw axis of the motion, and each $\dot{\theta}_n$ is the magnitude of the angular velocity about the axis. By rewriting Eq. (5) into a matrix form, we can assemble the Jacobian matrix ${}^n J$ in frame $\{n\}$ as

$$\begin{aligned} {}^n [{}^0 \underline{t}_n] &= {}^n J(\eta) \dot{\eta} \\ &= \begin{bmatrix} {}^n [{}^0 \underline{t}_1] {}^n [{}^1 \underline{t}_2] \cdots {}^n [{}^{n-2} \underline{t}_{n-1}] {}^n [{}^{n-1} \underline{t}_n] \end{bmatrix} \begin{bmatrix} \dot{\theta}_1 \\ \dot{\theta}_2 \\ \vdots \\ \dot{\theta}_{n-1} \\ \dot{\theta}_n \end{bmatrix}. \end{aligned} \quad (6)$$

3.2. Types of mobile manipulator modules

We consider a mobile manipulator as being composed of two subsystems—(a) a *differentially driven wheeled mobile robot* (WMR) platform, and (b) a *three-DOF serial manipulator* mounted at the midpoint of the axle between the two driving wheels as shown in Fig. 2. We note that the revolute (R) and the prismatic (P) joints are the only two possibilities for lower-pair joints that can enforce planar motion in

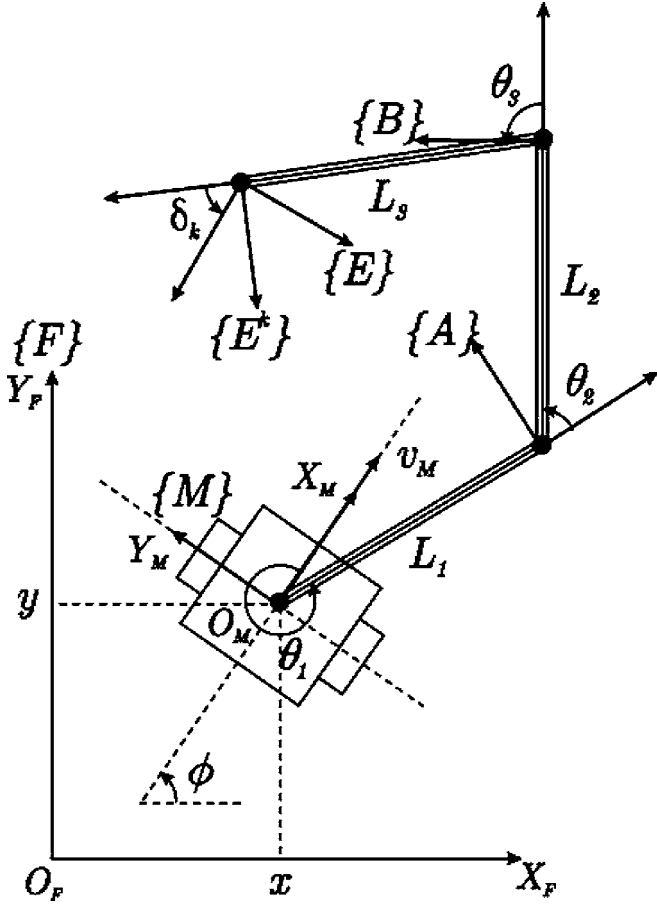


Fig. 2. Kinematic model of individual wheeled mobile manipulator module.

Table I. Eight possible combinations of simple three-degree of freedom planar manipulator with revolute (R) and prismatic joints (P). The PPP configuration does not allow arbitrary orientation of the end-effector.

RRR	PRR
RRP	PRP
RPR	PPR
RPP	PPP

the mounted manipulator. Thus, only eight potential configurations of a three-DOF serial manipulator can be created by combinations of the three revolute/prismatic joints, as shown in Table I. Further, some of these configurations (such as PPP configuration) do not even yield the desired full three DOF in the plane between the base and end-effector.

In this paper, we restrict our attention to the RRR configuration for the mounted manipulator atop a nonholonomic wheeled base to form the so-called NH-RRR-type mobile manipulator module. While heterogeneity of modules used to form the composite system can potentially yield greater variability, we focus on creating the composite cooperating system using three identical/homogeneous NH-RRR-type mobile manipulator modules. This intentional narrowing

of focus now facilitates the comparative study of the configuration dependence of the three-module system with other three-RRR planar parallel manipulator (albeit with fixed bases). In particular, it allows a systematic study of the role of the mobile bases on the overall system performance, especially in situations where these mobile bases feature nonholonomic constraints. Finally, this narrowing of focus does not prove too restrictive, since the selection of actuation can still create significant variability in performance (as we will systematically study later).

3.3. Twist modeling of the NH-RRR-type module

Referring to Fig. 2, frame $\{M\}$ is rigidly attached to the WMR with the X_M -axis oriented in the direction of the forward travel, and Y_M -axis oriented at the direction perpendicular to X_M -axis (i.e., the direction of the nonholonomic constraint). Frames $\{A^k\}$, $\{B^k\}$, and $\{E^k\}$ are rigidly attached to the distal ends of first, second, and third links, respectively. Without the loss of generality, we also consider that the body-fixed frame $\{E\}$ attached to the payload is offset with respect to the end-effector frame $\{E^k\}$, by a constant offset angle δ_k . The configuration of the manipulator with the three revolute joints can be parameterized by the three relative angles θ_1 , θ_2 , and θ_3 , with the link lengths L_1 , L_2 , and L_3 . Note that the third link is a virtual link that connects the point of attachment of the payload (origin of frame $\{B\}$) to the origin of the payload reference frame $\{E\}$. The configuration of the WMR can be described as

$${}^F A_M = \begin{bmatrix} \cos \phi & -\sin \phi & x \\ \sin \phi & \cos \phi & y \\ 0 & 0 & 1 \end{bmatrix}. \quad (7)$$

The body-fixed twist matrix of the mobile robot ${}^M [{}^F T_M]$ is obtained as

$${}^M [{}^F T_M] = \begin{bmatrix} 0 & -\dot{\phi} & \dot{x} \cos \phi + \dot{y} \sin \phi \\ \dot{\phi} & 0 & -\dot{x} \sin \phi + \dot{y} \cos \phi \\ 0 & 0 & 0 \end{bmatrix} \quad (8)$$

where $\dot{\phi} = \omega_M$ is the angular velocity of the mobile robot. By noting that $-\dot{x} \sin \phi + \dot{y} \cos \phi = 0$ and that $\dot{x} \cos \phi + \dot{y} \sin \phi$ can be expressed as the forward velocity v_M , we can obtain a parameterization of the total twist in terms of $\dot{\phi}$ and v_M as

$${}^M [{}^F T_M] = \underbrace{{}^M \begin{bmatrix} 0 & -1 & 0 \\ 1 & 0 & 0 \\ 0 & 0 & 0 \end{bmatrix}}_{{}^M [T_{\dot{\phi}}]} \dot{\phi} + \underbrace{{}^M \begin{bmatrix} 0 & 0 & 1 \\ 0 & 0 & 0 \\ 0 & 0 & 0 \end{bmatrix}}_{{}^M [T_{v_M}]} v_M. \quad (9)$$

The corresponding twist vectors as expressed in the common payload frame $\{E\}$ can be written as

$${}^E [{}^F \underline{t}_M] = {}^E [\underline{t}_{\omega_M}] \omega_M + {}^E [\underline{t}_{v_M}] v_M \quad (10)$$

where

$${}^E[\underline{t}_{\omega_M}] = \begin{bmatrix} 1 \\ -L_1 \sin(\delta_k - \theta_2 - \theta_3) - L_2 \sin(\delta_k - \theta_3) - L_3 \sin \delta_k \\ L_1 \cos(\delta_k - \theta_2 - \theta_3) + L_2 \cos(\delta_k - \theta_3) + L_3 \cos \delta_k \end{bmatrix} \quad (11)$$

$${}^E[\underline{t}_{v_M}] = \begin{bmatrix} 0 \\ \cos(\delta_k - \theta_1 - \theta_2 - \theta_3) \\ \sin(\delta_k - \theta_1 - \theta_2 - \theta_3) \end{bmatrix}. \quad (12)$$

Similarly, the twist at the end-effector of the serial manipulator can be expressed as a linear combination of the twist contributions of each revolute joint as

$${}^E[{}^M \underline{t}_E] = {}^E[\underline{t}_{\dot{\theta}_1}] \dot{\theta}_1 + {}^E[\underline{t}_{\dot{\theta}_2}] \dot{\theta}_2 + {}^E[\underline{t}_{\dot{\theta}_3}] \dot{\theta}_3 \quad (13)$$

where

$${}^E[\underline{t}_{\dot{\theta}_1}] = \begin{bmatrix} 1 \\ -L_1 \sin(\delta_k - \theta_2 - \theta_3) - L_2 \sin(\delta_k - \theta_3) - L_3 \sin \delta_k \\ L_1 \cos(\delta_k - \theta_2 - \theta_3) + L_2 \cos(\delta_k - \theta_3) + L_3 \cos \delta_k \end{bmatrix} \quad (14)$$

$${}^E[\underline{t}_{\dot{\theta}_2}] = \begin{bmatrix} 1 \\ -L_2 \sin(\delta_k - \theta_3) - L_3 \sin \delta_k \\ L_2 \cos(\delta_k - \theta_3) + L_3 \cos \delta_k \end{bmatrix} \quad (15)$$

$${}^E[\underline{t}_{\dot{\theta}_3}] = \begin{bmatrix} 1 \\ -L_3 \sin \delta_k \\ L_3 \cos \delta_k \end{bmatrix}. \quad (16)$$

The end-effector twist can now be related to the various joint rates by way of a geometrically assembled Jacobian matrix as

$${}^E[{}^F \underline{t}_E] = {}^E J(\eta) \dot{\eta} = \begin{bmatrix} \omega_M \\ v_M \\ \dot{\theta}_1 \\ \dot{\theta}_2 \\ \dot{\theta}_3 \end{bmatrix}. \quad (17)$$

Such a modular assembly of the Jacobian matrix is useful as has been explored further in the subsequent sections. For the remainder of the paper, we denote the end-effector twist ${}^E \underline{t}$ instead of ${}^E[{}^F \underline{t}_E]$.

4. Modeling of Composite Cooperating System

Multiple kinematic closed-loop constraints are formed when the common payload is placed on the end-effectors of adjacent cooperating mobile manipulator modules. We treat the payload as a common reference member of Type 0 simple-closed-chain system and the various mobile manipulator modules as the serial-chain legs. For this paper, we also assume that a rigid connection is formed between the payload and the end-effector, i.e., all mobility at the contact is localized within the attaching serial-chain. However, we note that it is possible to model a variety of other grasping conditions^{38,39} (from frictionless hard point contacts to soft finger contacts with friction) within this formulation relatively easily.

Let the complete set of joint velocities of the constrained mechanical system be described by a vector of the generalized velocities $\dot{\eta}$. The differential-kinematic model of the closed-loop constrained system can generally be written as

$$J_T(\eta) \dot{\eta} = {}^E \underline{t} \quad (18)$$

subject to the general velocity-level constraint equations

$$J_C(\eta) \dot{\eta} = \underline{0}. \quad (19)$$

The number of independent loops that forms the Jacobian matrix $J_C(\eta)$ can be determined by the Euler equation by viewing the system as a network (with the links as nodes and the joints as edges).⁴⁰ We note that within a parallel-chain mechanism, not all the joints in the system need to be actuated. The mixture of active and passive joint components can help partition the rate vector as $\eta^T = [\eta_a^T \ \eta_p^T]$. $\dot{\eta}_a$ and $\dot{\eta}_p$ are the subvectors of the active and passive manipulation rates variables within the entire constrained mechanical system. J_T and J_C can then be partitioned accordingly, permitting Eqs. (18) and (19) to be rewritten as

$$J_{T_a} \dot{\eta}_a + J_{T_p} \dot{\eta}_p = {}^E \underline{t} \quad (20)$$

$$J_{C_a} \dot{\eta}_a + J_{C_p} \dot{\eta}_p = \underline{0}. \quad (21)$$

A general solution of Eq. (21) for $\dot{\eta}_p$ can be determined as

$$\dot{\eta}_p = -J_{C_p}^+ J_{C_a} \dot{\eta}_a + \tilde{J}_{C_p} \xi \quad (22)$$

where the superscript “+” denotes the Moore–Penrose inverse of the matrix, \tilde{J}_{C_p} is the right annihilator of J_{C_p} , i.e., $J_{C_p} \tilde{J}_{C_p} = \underline{0}$, and ξ is any arbitrary vector parameterizing the nullspace of J_{C_p} . Using Eq. (22) with (20), we get

$$\begin{aligned} {}^E \underline{t} &= [J_{T_a} - J_{T_p} J_{C_p}^+ J_{C_a}] \dot{\eta}_a + J_{T_p} \tilde{J}_{C_p}^+ \xi \\ &= \tilde{J}_T \dot{\eta}_a + J_{T_p} \tilde{J}_{C_p}^+ \xi. \end{aligned} \quad (23)$$

\tilde{J}_T is the *system Jacobian matrix* that now relates the *actuated joint rates* of the system to the task space twists.

4.1. Actuation

Three different cases arise depending on the nature of the actuation within the system, which is reflected in the sizes of the matrices J_{C_a} and J_{C_p} .

4.1.1. Exact actuation. If the system is exactly actuated, as typically seen in parallel manipulators, then J_{C_p} has full rank and no longer possesses a nullspace. Thus, we can rewrite Eqs. (22) and (23) as

$$\dot{\eta}_p = -J_{C_p}^{-1} J_{C_a} \dot{\eta}_a \quad (24)$$

$${}^E \underline{t} = [J_{T_a} - J_{T_p} J_{C_p} J_{C_a}] \dot{\eta}_a = \bar{J}_T \dot{\eta}_a. \quad (25)$$

4.1.2. Redundant actuation. In a redundantly actuated system, J_{C_p} is a rectangular $m \times n$ matrix with $m > n$ for which \bar{J}_{C_p} does not exist and the Moore–Penrose pseudo-inverse that solves the problem in the least-squares sense, can be determined as

$$J_{C_p}^+ = (J_{C_p}^T J_{C_p})^{-1} J_{C_p}^T. \quad (26)$$

4.1.3. Underactuation. In underactuated systems, J_{C_p} is generally a rectangular $m \times n$ matrix with $m < n$ and a nontrivial \bar{J}_{C_p} . The existence of the $J_{T_p} \bar{J}_{C_p}^+ \underline{\xi}$ term in Eq. (23) is unique to *underactuated closed-chain systems*. It corresponds to system *self-motion*, wherein the end-effector can still move even when all the active joints are locked. In order to prevent the self-motion, we choose to lock a selected number of the passive joints, as determined by the size of J_{C_p} . In this case, the size of \bar{J}_{C_p} is $n(n-m)$ with an $(n-m)$ -dimensional self-motion manifold, which necessitates locking of as many passive joints in order to eliminate all system self-motion. In terms of modeling, locking the passive joints entails eliminating the column vectors corresponding to the locked joints from J_{C_p} -such an elimination brings us back to an exactly actuated case.

4.2. Construction of system Jacobian matrix

For an N modules cooperative system, we denote each module $k = \text{I, II, } \dots, N$, and there are α -active and β -passive DOF in each module, the configuration of the cooperative system can be completely described by $N \cdot (\alpha + \beta)$ generalized coordinates. The generalized velocity can then be partitioned into

$$\dot{\eta}_a^T = [\{\dot{\eta}_a^{\text{I}}\}^T \quad \dots \quad \{\dot{\eta}_a^{\text{N}}\}^T] \quad (27)$$

$$\dot{\eta}_p^T = [\{\dot{\eta}_p^{\text{I}}\}^T \quad \dots \quad \{\dot{\eta}_p^{\text{N}}\}^T] \quad (28)$$

where the subscripts a and p indicate active and passive joints, respectively.

The end-effector task equation can be obtained by designating Module I as the “leader” of the system and

setting contributions of other modules to zero. We can then determine J_{T_a} and J_{T_p} as

$$J_{T_a} = [J_a^{\text{I}} \quad 0_{3 \times m} \quad \dots \quad 0_{3 \times m}] \quad (29)$$

$$J_{T_p} = [J_p^{\text{I}} \quad 0_{3 \times n} \quad \dots \quad 0_{3 \times n}]. \quad (30)$$

We note that there are many ways to formulate the constraint Jacobian matrix J_{C_a} and J_{C_p} .⁴¹ We, however, use the velocity-level loop closure equations with respect to the “leader” to obtain

$$J_{C_a} = \begin{bmatrix} J_a^{\text{I}} & -J_a^{\text{II}} & 0_{3 \times m} & \dots & 0_{3 \times m} & 0_{3 \times m} \\ J_a^{\text{I}} & 0_{3 \times m} & -J_a^{\text{III}} & \dots & 0_{3 \times m} & 0_{3 \times m} \\ \vdots & \vdots & \vdots & \ddots & \vdots & \vdots \\ J_a^{\text{I}} & 0_{3 \times m} & 0_{3 \times m} & \dots & 0_{3 \times m} & -J_a^{\text{N}} \end{bmatrix} \quad (31)$$

$$J_{C_p} = \begin{bmatrix} J_p^{\text{I}} & -J_p^{\text{II}} & 0_{3 \times n} & \dots & 0_{3 \times n} & 0_{3 \times n} \\ J_p^{\text{I}} & 0_{3 \times n} & -J_p^{\text{III}} & \dots & 0_{3 \times n} & 0_{3 \times n} \\ \vdots & \vdots & \vdots & \ddots & \vdots & \vdots \\ J_p^{\text{I}} & 0_{3 \times n} & 0_{3 \times n} & \dots & 0_{3 \times n} & -J_p^{\text{N}} \end{bmatrix}. \quad (32)$$

4.3. Manipulability-based performance measure

In this paper, we focus only on the translational Jacobian mapping—the sub-matrix of the second and the third rows of the system Jacobian matrix \bar{J}_T , which we denote as $\bar{J}_{T,\text{tr}}$. The SVD of this matrix can now be used to examine the manipulability characteristics and its interpretation in the context of the manipulability ellipsoid geometry.

In our case, we adopt the *isotropy index* as the measure-of-choice to characterize the performance of our cooperative system. We summarize the evaluation of the isotropy index here, and refer the interested reader to refs. 34, 42 for descriptions of some of the benefits including boundedness and excellent numerical behavior. Let an $m \times n$ system Jacobian matrix be decomposed as

$$\bar{J}_{T,\text{tr}} = U \Sigma V^T \quad (33)$$

where the columns of the matrices $U_{m \times m}$ and $V_{n \times n}$ are, respectively, orthonormal eigenvectors of $[\bar{J}_{T,\text{tr}}][\bar{J}_{T,\text{tr}}]^T$ and $[\bar{J}_{T,\text{tr}}]^T[\bar{J}_{T,\text{tr}}]$. If the rank of $\bar{J}_{T,\text{tr}}$ is $k \leq \min(m, n)$, then

$$\Sigma_{m \times n} = \text{diag} \left(\underbrace{\sigma_1, \sigma_2, \dots, \sigma_k}_k, \underbrace{0, \dots, 0}_{n-k} \right), \sigma_1 \geq \sigma_2 \geq \dots \geq \sigma_k \quad (34)$$

where σ_i , $i = 1, 2, \dots, k$ are the singular values of $\bar{J}_{T,\text{tr}}$ ordered from the minimum to the maximum. Finally, we can define the isotropy index as

$$\Gamma_{I,\text{tr}} = \frac{\sigma_1}{\sigma_k}. \quad (35)$$

However, $\bar{J}_{T,\text{tr}}$ depends upon the selection of the actuated and unactuated joints. In subsequent sections, we examine some

of the different case studies that arise due to such selections of the type and location of the actuation.

5. Case studies

We consider the case of three mobile manipulators coming together in a formation to cooperatively transport a common payload. The individual modules are numbered *I*, *II*, and *III*, as depicted in Fig. 3. We denote the revolute joints $R1^k$, $R2^k$, and $R3^k$, and the mobile bases MB^k , where $k = I, II, III$. When an object is placed at the end-effectors of the mobile manipulator modules, it effectively creates a *mobile three-RRR planar parallel mechanism*. The three-module case permits us to provide linkage to some existing

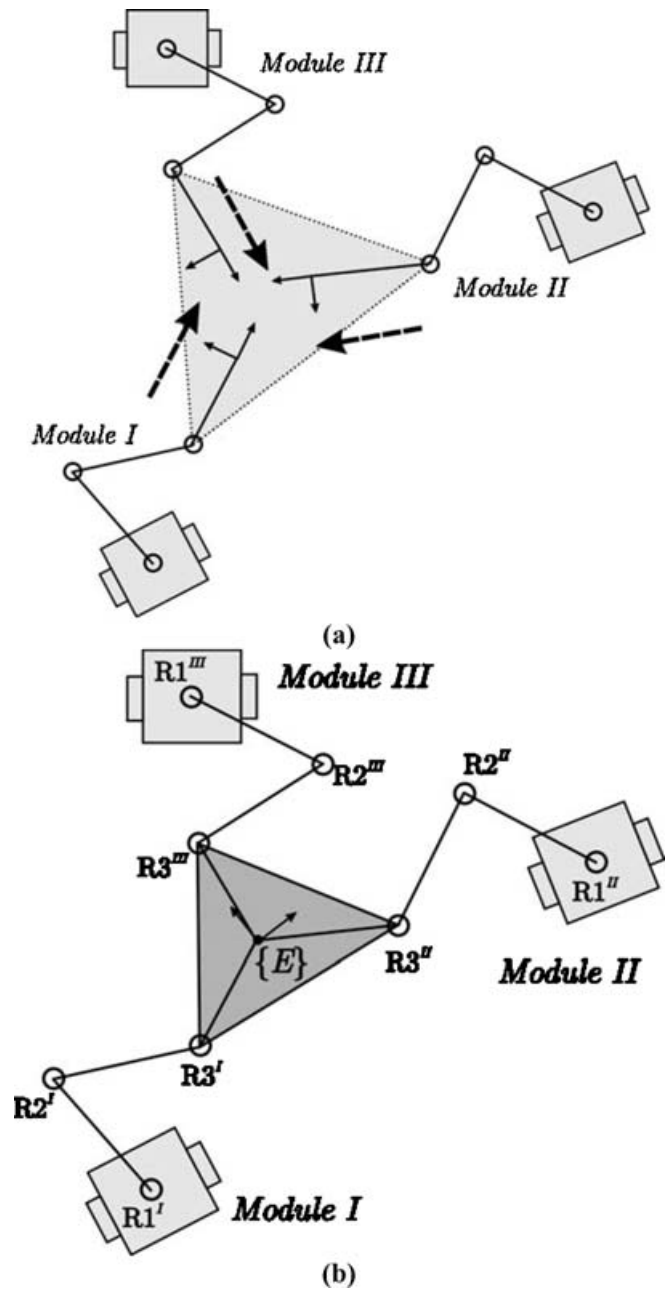


Fig. 3. Three mobile modules (a) attach together by placing a common payload to effectively form (b) a composite locomotion system.

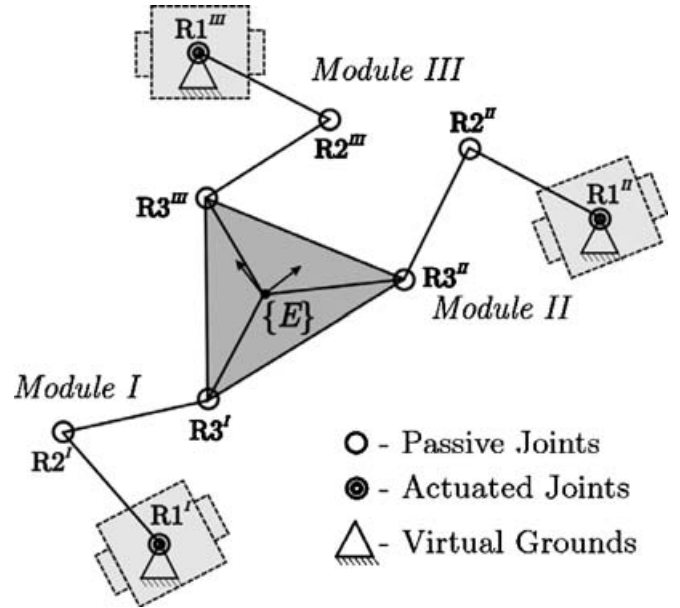


Fig. 4. Case I—Cooperative system with MB locked, R1 active, and R2 passive.

literature, for example, the stationary composite system is nothing more than the traditional *three-RRR planar parallel mechanism*.^{43,44}

Without the loss of generality, and for convenience of comparison with the existing literature, we impose some further design limitations. We require use of identical mobile modules, i.e., the mobile bases have the same size and the manipulators have the same link lengths. Further, we also impose a requirement for symmetry of actuation within the contributing subchains. Finally, note that the formulation can be extended to increasing numbers of modules as well as the various selections of actuator locations within the system. Twenty-seven permutations are possible based on whether MB, R1, and R2 are chosen to be locked, made passive, or made active. However, only five interesting sets of cases (depicted in Figs. 4–8) were selected for further study and are listed in Table II.

5.1. Study parameters

For our study, we locate the MBs at the vertices of an equilateral triangle of side 4 m, with the payload taking the form of another equilateral triangle of side 1.7321 m, as shown in Fig. 9. The end-effector frame is assumed to be located at the centroid of the payload-triangle with an orientation $\phi_E = 0^\circ$. The workspace area spanned by the mechanism is highly dependent on the dimensions of the

Table II. Five candidate cases based on the actuation-status of the joints within each chain.

Cases	MB	R1	R2
I	Locked	Active	Passive
II	Locked	Passive	Active
III	Active	Passive	Passive
IV	Active	Locked	Passive
V	Active	Passive	Locked

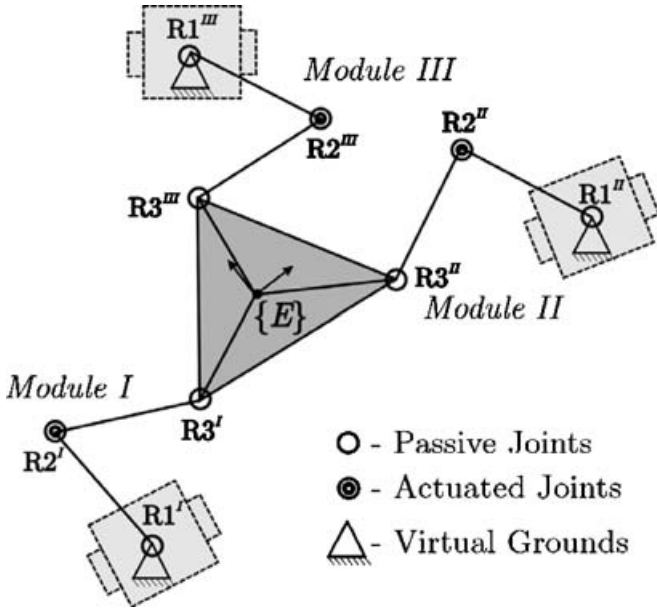


Fig. 5. Case II—Cooperative system with MB locked, R1 passive, and R2 active.

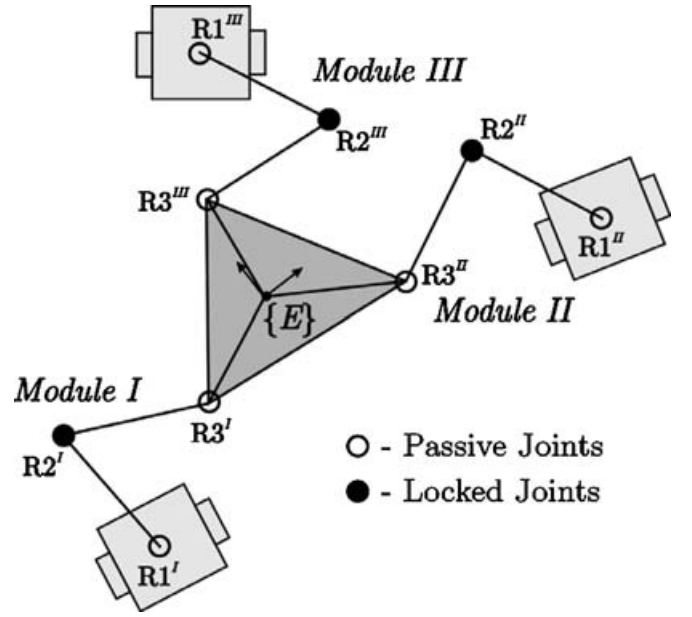


Fig. 7. Case IV—Cooperative system with MB active, R1 locked, and R2 passive.

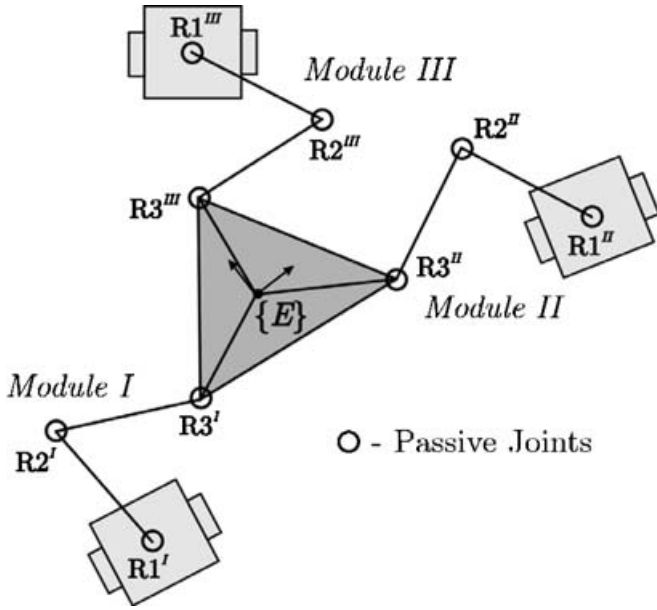


Fig. 6. Case III—Cooperative system with MB active, R1 passive, and R2 passive.

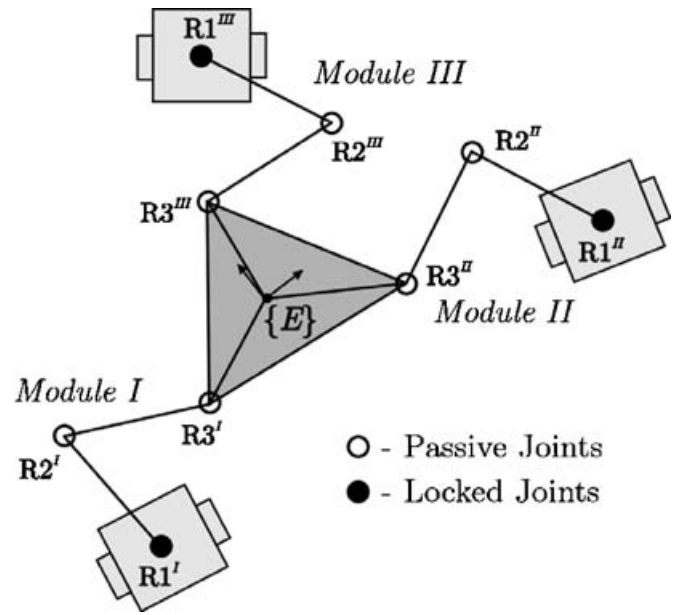


Fig. 8. Case V—Cooperative system with MB active, R1 passive, and R2 locked.

links, and by imposing a design criterion that $L_1^k = L_2^k$ for the modules, we can realize a symmetrical workspace, without any unreachable regions.³ The other critical dimensions are shown in Table III. However, the mechanism has eight working modes with different elbow configurations. We denote 0 and 1 for elbow up and elbow down configuration, respectively. Individual assembly mode can be identified as abc , $\forall a, b, c \in \{0, 1\}$. We assume the elbow configuration of 111 throughout the paper. We compute the isotropy index, bounded between 0 and 1, over the entire *feasible* workspace on a 100×100 grid with spacing of 0.004 m and show these results in the form of pseudo-color, contour, and surface plots (Table III).

Table III. Detailed study parameters.

Link lengths (m)	Base positions (m)	Platform offset angles ($^\circ$)
$L_1^k = 1.5$	$(x_1^I, y_1^I) = (0, 0)$	$\delta^I = 330$
$L_2^k = 1.5$	$(x_1^{II}, y_1^{II}) = (3.4641, 2)$	$\delta^{II} = 210$
$L_3^k = 1$	$(x_1^{III}, y_1^{III}) = (0, 4)$	$\delta^{III} = 90$

5.1.1. Case I: MB locked, R1 active, R2 passive. In this case, the mobile base of each module is locked in place and the joint R1 of each module is actuated, creating

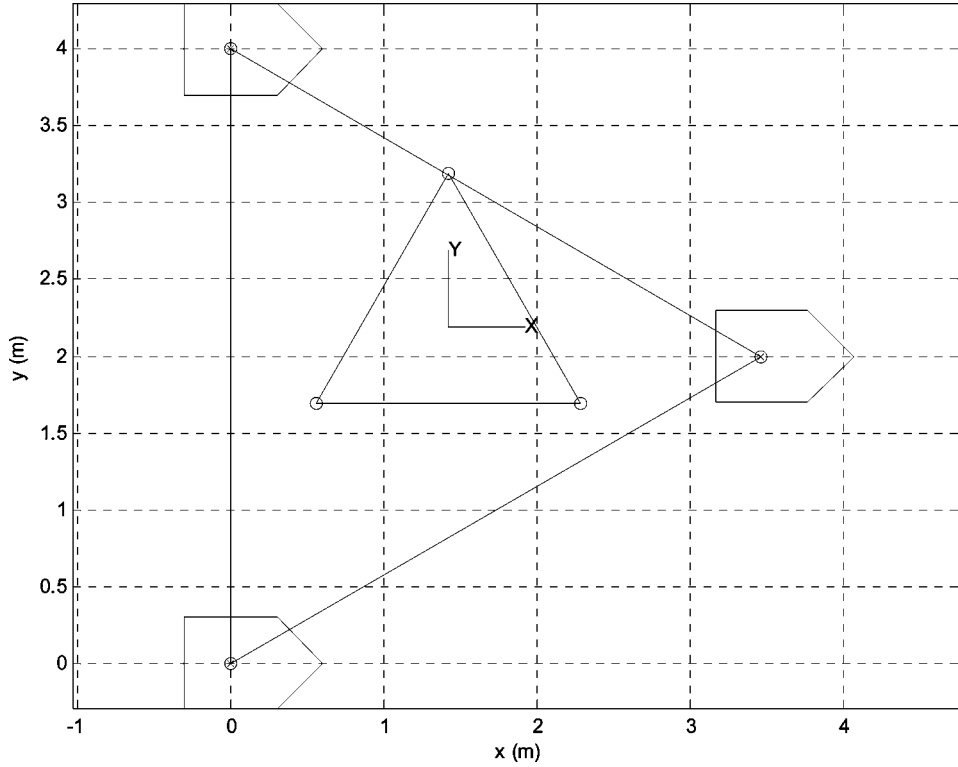


Fig. 9. Location of the mobile bases and the geometry of the platform.

a stationary three-RRR¹ planar parallel manipulator, as seen in Fig. 4. This case was interesting from two viewpoints: First, it allows us to validate the formulation and results with the existing literature.^{43,45,46} Second, and more importantly, such a system results when the mobile bases are brought to a temporary halt and a relative manipulation/reconfiguration of the payload with respect to the bases is pursued. In this case, the active manipulation rates are $\dot{\eta}_a = [\dot{\theta}_1^I \ \dot{\theta}_1^{II} \ \dot{\theta}_1^{III}]^T$, and passive manipulation rates are $\dot{\eta}_p = [\dot{\theta}_2^I \ \dot{\theta}_3^I \ \dot{\theta}_2^{II} \ \dot{\theta}_3^{II} \ \dot{\theta}_2^{III} \ \dot{\theta}_3^{III}]^T$. As seen in Fig. 10, the plots of the isotropy index are symmetric with the highest value occurring at the center of the workspace (the centroid of the triangle formed by the MBs). However, it is important to note that this surface would be different for each of the eight kinematically distinct working modes.⁴³

5.1.2. Case II: MB locked, R1 passive, R2 active. In this case, the mobile base of each module is again kept fixed, but we actuate R2 of each module instead of R1. This results in the stationary three-RRR planar parallel manipulator shown in Fig. 5. This enables us to see how the isotropy index surface changes with an alternate actuation scheme. In this case, the active manipulation rates are $\dot{\eta}_a = [\dot{\theta}_2^I \ \dot{\theta}_2^{II} \ \dot{\theta}_2^{III}]^T$, and $\dot{\eta}_p = [\dot{\theta}_1^I \ \dot{\theta}_3^I \ \dot{\theta}_1^{II} \ \dot{\theta}_3^{II} \ \dot{\theta}_1^{III} \ \dot{\theta}_3^{III}]^T$ form the passive manipulation rates. The computed isotropy index over the feasible workspace is depicted in Fig. 11. In the plots, we can see that although the geometrical (structural) properties of the mechanisms are the same as in the previous case, changing the location of the actuation alter the isotropy index distribution. As in

¹ The underline under the first ‘‘R’’ indicates that the first joint of each manipulator chain is actuated.

the previous case, the workspace is symmetrical with same elbow configuration in each module. Again we also observe that the isotropy index is symmetrical with the highest value occurring at the centroid of the triangle formed by the MBs. While the mechanism has eight working modes, they are all kinematically identical and hence we obtain the same isotropy index plots in all working modes.⁴³

Finally, we realize that both stationary three-RRR and three-RRR manipulators have a limited workspace. The mobility of the bases can be used to create a locomoting structure in order to extend the workspace to include the entire plane.

5.1.3. Case III: MB active, R1 passive, R2 passive. In this case, we allow the mobile base to move and free-up all the other joints within the arm as shown in Fig. 6. The active rates and passive rates can be selected as $\dot{\eta}_a = [\dot{\phi}^I \ v_M^I \ \dot{\phi}^{II} \ v_M^{II} \ \dot{\phi}^{III} \ v_M^{III}]^T$ and $\dot{\eta}_p = [\dot{\theta}_1^I \ \dot{\theta}_2^I \ \dot{\theta}_3^I \ \dot{\theta}_1^{II} \ \dot{\theta}_2^{II} \ \dot{\theta}_3^{II} \ \dot{\theta}_1^{III} \ \dot{\theta}_2^{III} \ \dot{\theta}_3^{III}]^T$.

The Jacobian matrices are independent of the pose of the mobile bases with respect to the inertial-fixed frame, but dependent on their pose relative to the end-effector frame. Thus, the benefit of formulating the Jacobian matrices of the locomotion system in the end-effector frame becomes evident here. In this case, J_{C_p} is 6×9 , so this system is underconstrained. Hence, we need to lock $9 - 6 = 3$ joints in the system in order to eliminate all self-motion, which leads us to explore these last two cases.

5.1.4. Case IV: MB active, R1 locked, R2 passive. Referring to Fig. 7, the active manipulation rates are $\dot{\eta}_a = [\dot{\phi}^I \ v_M^I \ \dot{\phi}^{II} \ v_M^{II} \ \dot{\phi}^{III} \ v_M^{III}]^T$ and the passive manipulation

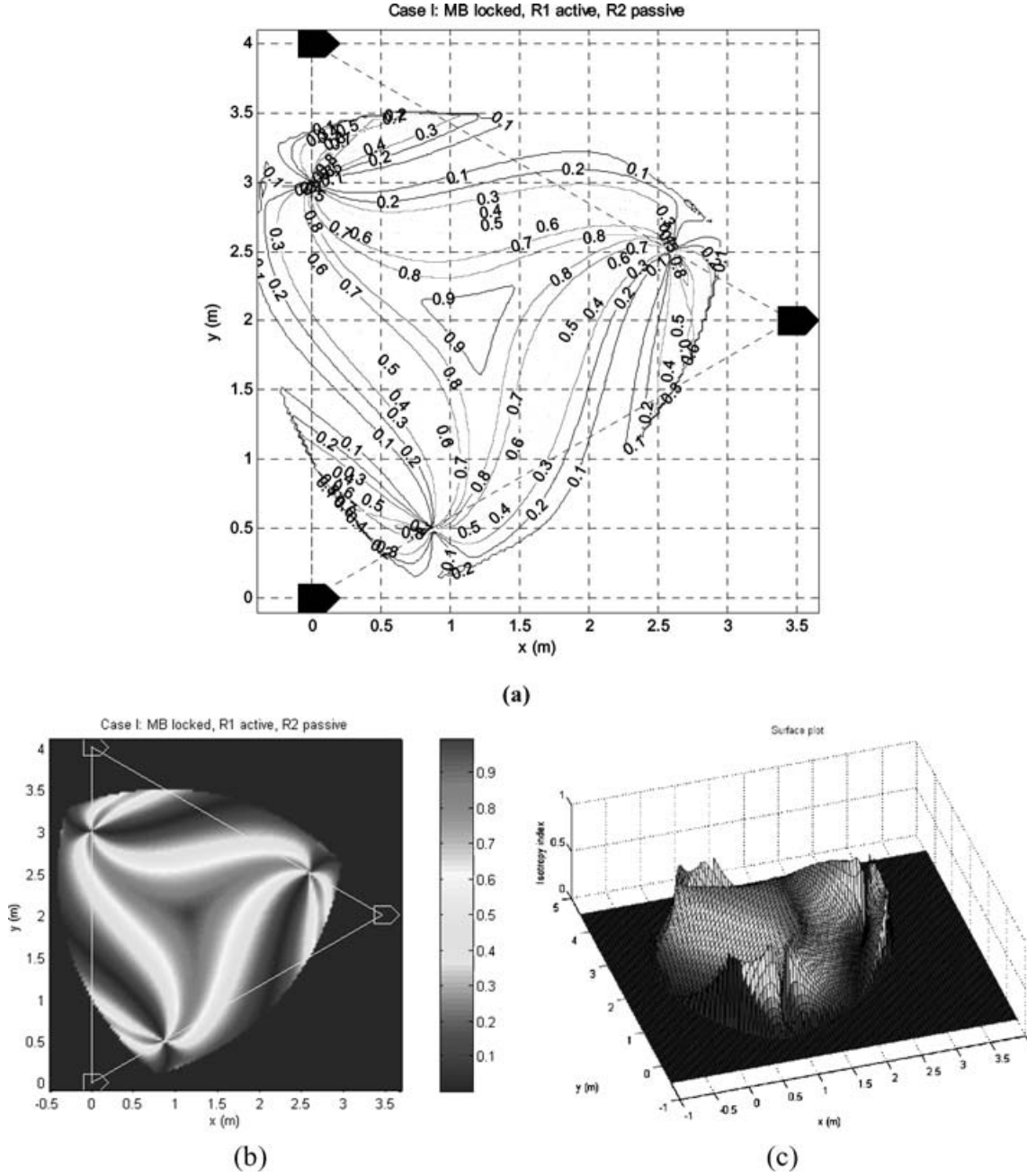


Fig. 10. Isotropy index plots for three-RRR planar parallel mechanism in Case I: (a) pseudo-color plot, (b) contour plot, and (c) surface plot.

rates are $\dot{\eta}_p = [\dot{\theta}_2^I \dot{\theta}_3^I \dot{\theta}_2^{II} \dot{\theta}_3^{II} \dot{\theta}_2^{III} \dot{\theta}_3^{III}]^T$. The corresponding Jacobian matrices are

$$J_{T_a} = \begin{bmatrix} {}^E t_{\phi}^I & {}^E t_{v_M}^I & \mathbf{0} & \mathbf{0} & \mathbf{0} & \mathbf{0} \end{bmatrix} \quad (36)$$

$$J_{T_p} = \begin{bmatrix} {}^E t_{\theta_2}^I & {}^E t_{\theta_3}^I & \mathbf{0} & \mathbf{0} & \mathbf{0} & \mathbf{0} \end{bmatrix} \quad (37)$$

$$J_{C_a} = \begin{bmatrix} {}^E t_{\phi}^I & {}^E t_{v_M}^I & -{}^E t_{\phi}^{II} & -{}^E t_{v_M}^{II} & \mathbf{0} & \mathbf{0} \\ {}^E t_{\phi}^I & {}^E t_{v_M}^I & \mathbf{0} & \mathbf{0} & -{}^E t_{\phi}^{III} & -{}^E t_{v_M}^{III} \end{bmatrix} \quad (38)$$

$$J_{C_p} = \begin{bmatrix} {}^E t_{\theta_2}^I & {}^E t_{\theta_3}^I & -{}^E t_{\theta_2}^{II} & -{}^E t_{\theta_3}^{II} & \mathbf{0} & \mathbf{0} \\ {}^E t_{\theta_2}^I & {}^E t_{\theta_3}^I & \mathbf{0} & \mathbf{0} & -{}^E t_{\theta_2}^{III} & -{}^E t_{\theta_3}^{III} \end{bmatrix} \quad (39)$$

As noted earlier, the MBs are instantaneously located at their current positions but are actuated. Hence, they contribute to the overall manipulability of the platform as can be seen from the isotropy index plots, shown in Fig. 12. In the plots, we note that the isotropy index surface plot is no longer symmetrical due to the nonholonomic constraints imposed by the MBs (in contrast to Case I). Further, the location of the peak of the isotropy index is no longer the centroid of the triangle formed by the MBs.

5.1.5. Case V: MB active, R1 passive, R2 locked. In this case, we would like to see the effect on the manipulability when locking different joints in the system. Referring to Fig. 8, we allow the MBs to move but lock the joints R2 in each module. The active manipulation rates are $\dot{\eta}_a = [\dot{\phi}^I v_M^I \dot{\phi}^{II} v_M^{II} \dot{\phi}^{III} v_M^{III}]^T$ and passive manipulation rates are

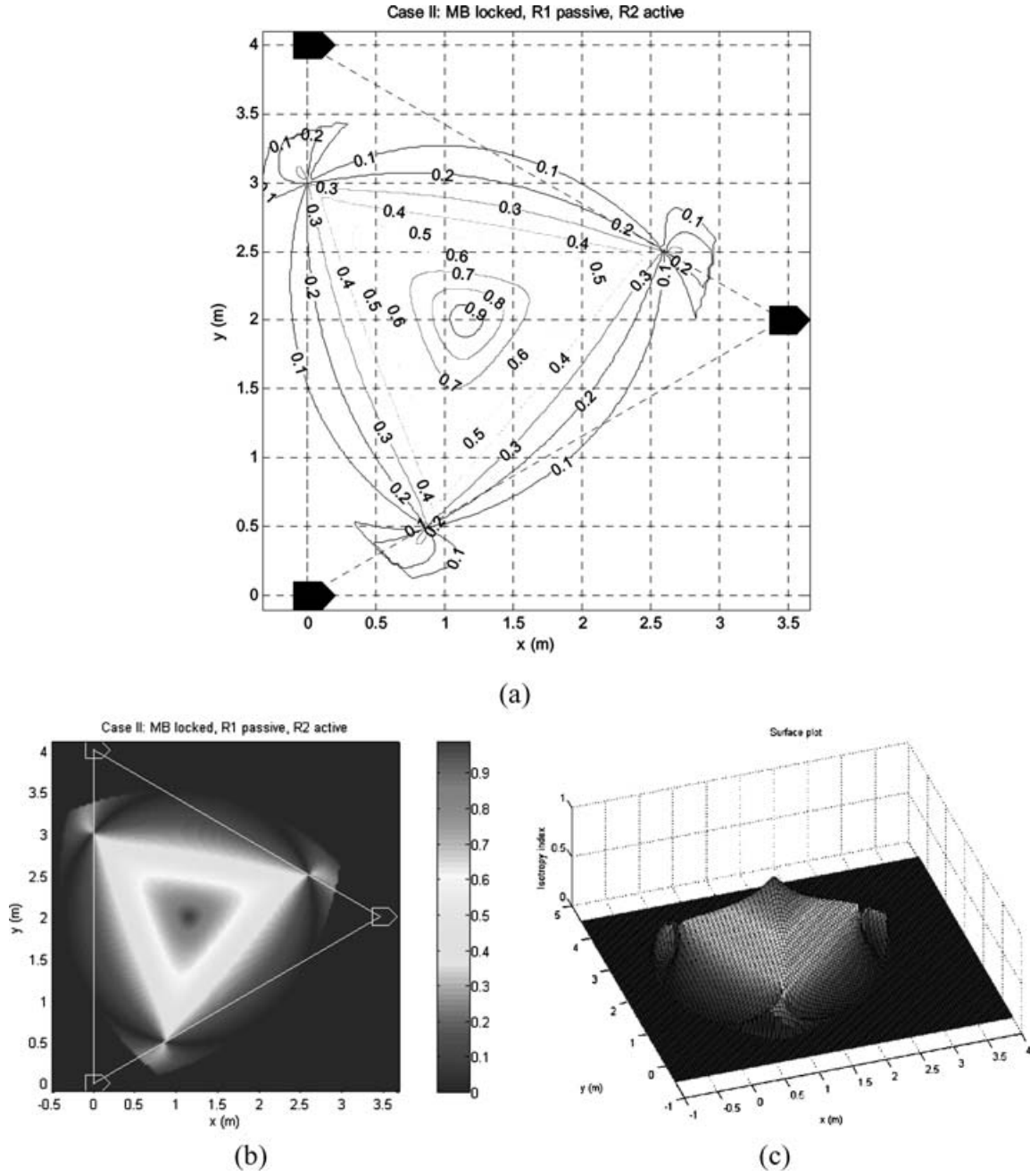


Fig. 11. Isotropy index plots for three-RRR planar parallel mechanism in Case II: (a) pseudo-color plot, (b) contour plot, and (c) surface plot.

$\dot{y}_p = [\dot{\theta}_1^I \ \dot{\theta}_3^I \ \dot{\theta}_1^{II} \ \dot{\theta}_3^{II} \ \dot{\theta}_1^{III} \ \dot{\theta}_3^{III}]^T$. The corresponding Jacobian matrices are

$$J_{T_a} = \begin{bmatrix} E \underline{t}_{\phi}^I & E \underline{t}_{v_M}^I & \mathbf{0} & \mathbf{0} & \mathbf{0} & \mathbf{0} \end{bmatrix} \quad (40)$$

$$J_{T_p} = \begin{bmatrix} E \underline{t}_{\theta_1}^I & E \underline{t}_{\theta_3}^I & \mathbf{0} & \mathbf{0} & \mathbf{0} & \mathbf{0} \end{bmatrix} \quad (41)$$

$$J_{C_a} = \begin{bmatrix} E \underline{t}_{\phi}^I & E \underline{t}_{v_M}^I & -E \underline{t}_{\phi}^{II} & -E \underline{t}_{v_M}^{II} & \mathbf{0} & \mathbf{0} \\ E \underline{t}_{\phi}^I & E \underline{t}_{v_M}^I & \mathbf{0} & \mathbf{0} & -E \underline{t}_{\phi}^{III} & -E \underline{t}_{v_M}^{III} \end{bmatrix} \quad (42)$$

$$J_{C_p} = \begin{bmatrix} E \underline{t}_{\theta_1}^I & E \underline{t}_{\theta_3}^I & -E \underline{t}_{\theta_1}^{II} & -E \underline{t}_{\theta_3}^{II} & \mathbf{0} & \mathbf{0} \\ E \underline{t}_{\theta_1}^I & E \underline{t}_{\theta_3}^I & \mathbf{0} & \mathbf{0} & -E \underline{t}_{\theta_1}^{III} & -E \underline{t}_{\theta_3}^{III} \end{bmatrix}. \quad (43)$$

The plots of the isotropy index are shown in Fig. 13. In the plots, we see that locking different joints changes the manipulability characteristic in contrast with Case IV (and with the Case II discussed earlier).

6. Conclusion

In this paper, we treated the cooperating system as a Type 0 constrained system and leveraged the modeling framework of constrained articulated mechanical system to create a unified kinematic system model. This framework takes the nonholonomic constraints, kinematic loop-closure constraints, and mixtures of active, locked, and passive joints into account explicitly. System-level performance measures are developed for the overall cooperating system, in terms of

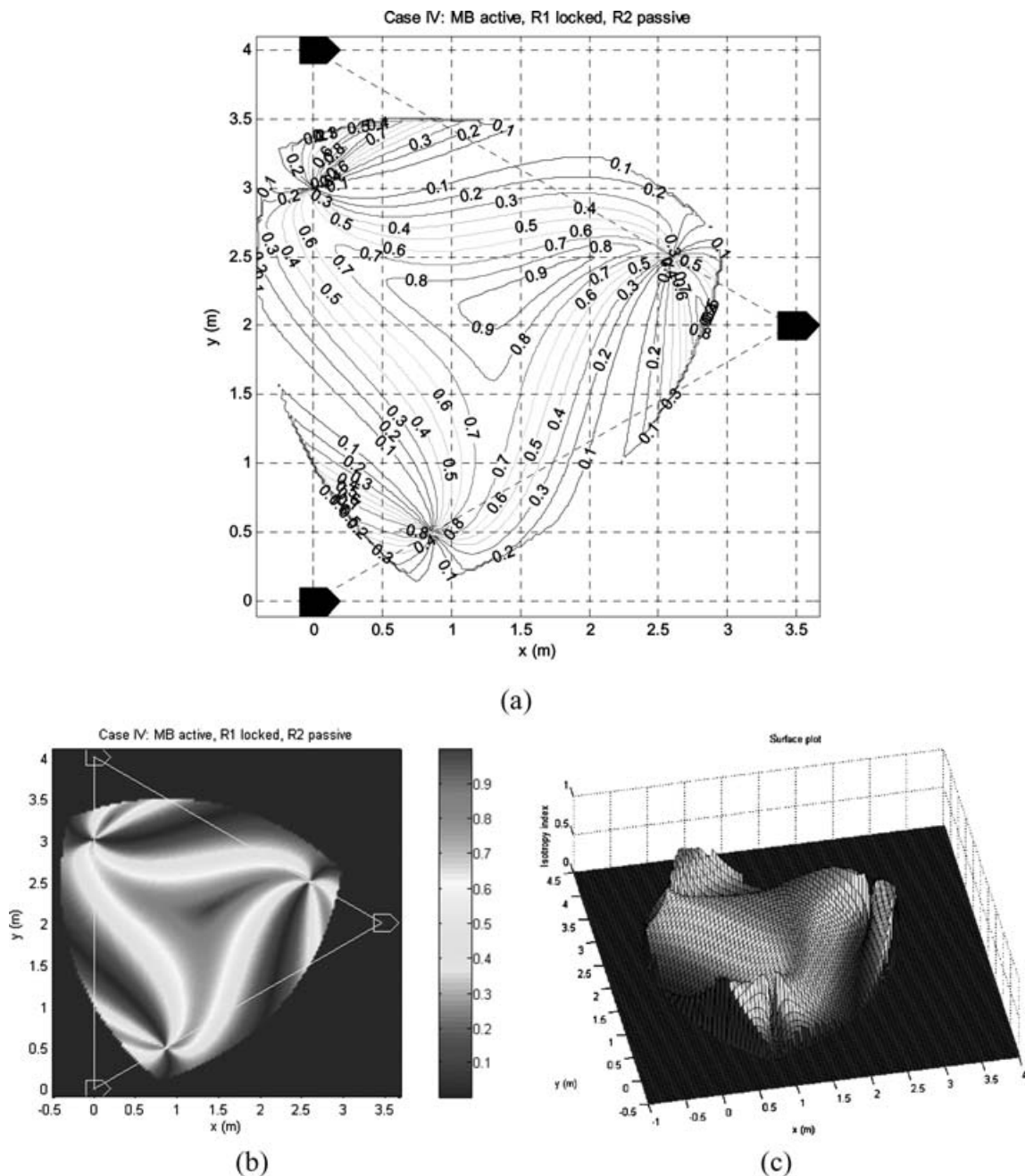


Fig. 12. Isotropy index plots for the mobile planar three-RRR parallel mechanism with R1 locked in Case IV: (a) pseudo-color plot, (b) contour plot, and (c) surface plot.

the system-level Jacobian matrix, which allows us to compare a number of case scenarios. High values of the isotropy index at a point or over a region of the configuration-space of the system indicate the payload is equally manipulable in every direction in the plane. In general, we observed that all three factors (a) the holonomic constraints due to the kinematic closed loops, (b) the existence of nonholonomic constraint due to the disk wheels, and (c) selection of actuations of the various joints, affected the performance of the cooperative system.

However, in this paper, we focused on the role of the latter two—the nonholonomic constraints and the joint actuation—on system performance. We note that the wheeled mobile bases facilitated the creation of the locomotive structure, and thereby extended the overall workspace. In addition, the

overall resulting values of the isotropy index were higher than the case where the bases are fixed but affected the symmetry of the isotropy index surface. The designer also has the capability of selectively actuating, locking, or rendering passive the various joints within the system. The case studies using the mobile three-RRR planar manipulator configuration permitted us to study the effect of different actuation schema on the isotropy index surface *systematically*. In general, from the viewpoint of system implementation, it may be preferable to actuate the proximal joints and leave the more distal joints passive or locked. However, the case studies clearly portray the greater influence of actuation of the distal joints on ensuring higher values and a more uniform distribution of the isotropy index. Finally, we also note that optimization-based methods may be used to determine sets

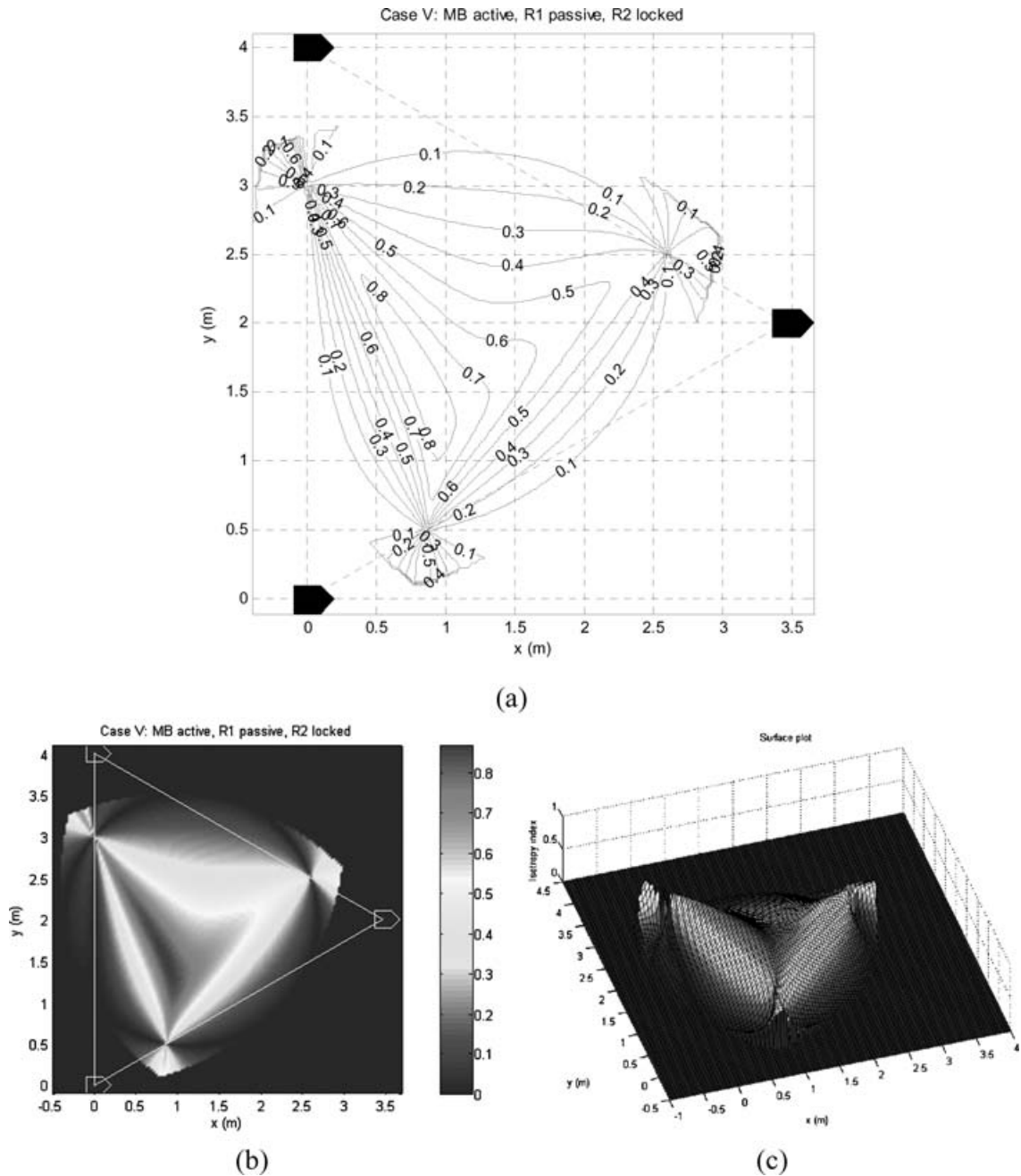


Fig. 13. Isotropy index plots for the mobile three-RRR parallel mechanism with R2 locked in Case V: (a) pseudo-color plot, (b) contour plot, and (c) surface plot.

of optimal system configurations that retain high values of the isotropy index along a given trajectory or over an entire region, but these are not reported here.^{3,31}

Acknowledgments

The authors gratefully acknowledge the support from the Research Foundation of the State University of New York and the National Science Foundation CAREER Award (IIS-0347653) for this research effort.

References

1. J. Adams, R. Bajcsy, J. Kosecka, V. Kumar, R. Mandelbaum, M. Mintz, R. Paul, C.-C. Wang, Y. Yamamoto and X. Yun, "Cooperative material handling by human and robotic agents: Module development and system synthesis," *Expert Syst. Appl.* **11**(2), 89–97 (1996).
2. M. Abou-Samah, *A Kinematically Compatible Framework for Collaboration of Multiple Non-holonomic Wheeled Mobile Robots* (Department of Mechanical Engineering, Center of Intelligent Machines, McGill University, Montreal, Canada, 2001).
3. C. P. Tang, *Manipulability-Based Analysis of Cooperative Payload Transport by Robot Collectives* (Department of Mechanical and Aerospace Engineering, University at Buffalo, Buffalo, NY, 2004).
4. R. C. Arkin and G. A. Bekey, *Robot Colonies* (Kluwer Academic, Boston, MA, 1997).
5. Y. Cao, A. S. Fukunaga and A. B. Kahng, "Cooperative mobile robotics: Antecedents and directions," *Auton. Robots* **4**(1), 7–27 (1997).

6. W. A. Khan, Distributed Dynamics of Systems with Closed Kinematic Chains (Department of Mechanical Engineering, McGill University, Montreal, QC, 2002).
7. J. Kerr and B. Roth, "Analysis of multifingered hands," *Int. J. Robot. Res.* **4**(4), 3–17 (1986).
8. J. K. Salisbury and J. J. Craig, "Articulated hands: Force control and kinematic issues," *Int. J. Robot. Res.* **1**(1), 4–17 (1982).
9. V. Kumar and K. J. Waldron, "Force distribution in closed kinematic chains," *IEEE Trans. Robot. Autom.* **4**(6), 657–664 (1988).
10. S. M. Song and K. J. Waldron, *Machines That Walk* (MIT, Cambridge, MA, 1989).
11. K. W. Lilly, *Efficient Dynamic Simulation of Robotic Mechanisms* (Kluwer Academic, Norwell, MA, 1993).
12. O. Khatib, K. Yokoi, K. Chang, D. Ruspini, R. Holmberg and A. Casal, "Vehicle/arm coordination and multiple mobile manipulator decentralized cooperation," Proceedings of the 1996 IEEE/RSJ International Conference on Intelligent Robots and Systems (1996) pp. 546–553.
13. J. P. Desai, J. P. Ostrowski and V. Kumar, "Modeling and control of formations of nonholonomic mobile robots," *IEEE Trans. Robot. Autom.* **17**(6), 905–908 (2001).
14. H. G. Tanner, K. J. Kyriakopoulos and N. I. Krikelias, "Modeling of multiple mobile manipulators handling a common deformable object," *J. Robot. Syst.* **15**(11), 599–623 (1998).
15. K. Kosuge, T. Osumi, M. Sato, K. Chiba and K. Takeo, "Transportation of a single object by two decentralized-controlled nonholonomic mobile robots," *Proceedings of the 1998 IEEE International Conference on Robotics and Automation* (1998) **4**, pp. 2989–2994.
16. M. Yamakita and J.-H. Suh, "Adaptive generation of desired velocity field for leader-follower type cooperative mobile robots with decentralized PVFC," *Proceedings of the 2001 IEEE International Conference on Robotics and Automation* (2001) **4**, pp. 3495–3502.
17. J. Desai and V. Kumar, "Motion planning for cooperating mobile manipulators," *J. Robot. Syst.* **16**(10), 557–579 (1999).
18. P. S. Krishnaprasad and D. P. Tsakiris, "Oscillations SE(2)-Snakes and motion control," *Proceedings of the 34th IEEE Conference on Decision and Control* (1995) pp. 2806–2811.
19. J. P. Ostrowski, *The Mechanics and Control of Undulatory Robotic Locomotion* (California Institute of Technology, Pasadena, CA, 1995).
20. J. Borenstein, B. Everett and L. Feng, *Navigating Mobile Robots: Systems and Techniques* (A. K. Peters, Wellesley, MA, 1996).
21. G. Campion, G. Bastin and B. D'Andrea-Novell, "Structural properties and classification of kinematic and dynamic models of wheeled mobile robots," *IEEE Trans. Robot. Autom.* **12**(1), 47–62 (1996).
22. F. G. Pin and M. Killough, "A new family of omnidirectional and holonomic wheeled platforms for mobile robots," *IEEE Trans. Robot. Autom.* **10**(4), 480–489 (1994).
23. D. B. Reister and M. A. Unseren, "Position and constraint force control of a vehicle with two or more steerable drive wheels," *IEEE Trans. Robot. Autom.* **9**(6), 723–731 (1993).
24. S. V. Sreenivasan and K. J. Waldron, "Displacement analysis of an actively articulated wheeled vehicle configuration with extensions to motion planning on uneven terrain," *ASME J. Mech. Des.* **118**(2), 312–317 (1996).
25. R. Ben-Horin, M. Shoham and S. Djerassi, "Kinematic, dynamics and construction of a planarly actuated parallel robot," *Robot. Comput.-Integr. Manuf.* **14**(2), 163–172 (1998).
26. S. Shoval and M. Shoham, "Sensory redundant parallel mobile mechanism," *Proceedings of the 2001 IEEE International Conference on Robotics and Automation* (2001).
27. S. Shoval and M. Shoham, "Analysis of a parallel mobile robot for motion on uneven slippery surfaces," *Proceedings of the International Conference for Field and Service Robotics* (2003).
28. Y. Nakamura, *Advanced Robotics: Redundancy and Optimization* (Addison-Wesley, CA, 1991).
29. T. Balch, "Hierarchic social entropy: An information theoretic measure of robot group diversity," *In: Autonomous Robots 8* (Kluwer Academic, The Netherlands, 2000) pp. 209–237.
30. C. Belta and V. Kumar, "Optimal motion generation for groups of robots: A geometric approach," *ASME J. Mech. Des.* **126**(1), 63–70 (2004).
31. R. M. Bhatt, C. P. Tang and V. Krovci, "Geometric motion planning and formation optimization for a fleet of nonholonomic wheeled mobile robots," *Proceedings of the 2004 IEEE International Conference of Robotics and Automation*, 2004).
32. M. Zefran, V. Kumar and C. B. Croke, "On the generation of smooth three-dimensional rigid body motions," *IEEE Trans. Robot. Autom.* **14**(4), 576–589 (Aug. 1998).
33. T. Yoshikawa, "Manipulability of robotic mechanisms," *Int. J. Robot. Res.* **4**(2), 3–9 (1985).
34. K. E. Zanganeh and J. Angeles, "Kinematic isotropy and the optimum design of parallel manipulators," *Int. J. Robot. Res.* **16**(2), 185–197 (1997).
35. Y. Yamamoto and X. Yun, "Coordinating locomotion and manipulation of a mobile manipulator," *IEEE Trans. Autom. Control* **39**(6), 1326–1332 (1994).
36. A. Bicchi and D. Prattichizza, "Manipulability of cooperating robots with unactuated joints and closed-chain mechanisms," *IEEE Trans. Robot. Autom.* **16**(4), 336–345 (2000).
37. F. C. Park and J. W. Kim, "Manipulability of closed kinematic chains," *ASME J. Mech. Des.* **120**(4), (1998).
38. J. T.-Y. Wen and L. S. Wilfinger, "Kinematic manipulability of general constrained rigid multibody systems," *IEEE Trans. Robot. Autom.* **15**(3), 558–567 (1999).
39. R. Murray, Z. Li and S. Sastry, *A Mathematical Introduction to Robotic Manipulation* (CRC, Boca Raton, FL, 1993).
40. M. G. Mohamed and C. M. Gosselin, "Design and analysis of kinematically redundant parallel manipulators with configurable platforms," *IEEE Trans. Robot.* **21**(3), 277–287 (2005).
41. P. Chiacchio, S. Chiaverini, L. Sciavicco and B. Siciliano, "Global task space manipulability ellipsoids for multiple-arm system," *IEEE Trans. Robot. Autom.* **7**(5), 678–685 (Oct. 1991).
42. J. Angeles, *Fundamentals of Robotics Mechanical Systems: Theory, Methods and Algorithms* (Springer-Verlag, New York, NY, 2002).
43. I. A. Bonev, *Geometric Analysis of Parallel Mechanisms* (Department of Mechanical Engineering, Laval University, Quebec City, QC, 2002).
44. I. A. Bonev, D. Zlatanov and C. Gosselin, "Singularity analysis of 3-DOF planar parallel mechanisms via screw theory," *ASME J. Mech. Des.* **125**, 573–581 (2003).
45. V. K. Chan and I. Ebert-Uphoff, "Investigation of the deficiencies of parallel manipulators in singular configurations through the Jacobian nullspace," *Proceedings of the 2001 IEEE International Conference on Robotics and Automation* (2001) pp. 1313–1320.
46. O. Ma and J. Angeles, "Direct kinematics and dynamics of a planar 3-DOF parallel manipulator," *Adv. Des. Autom.* **3**, 313–320 (1989).
47. G. White, *Simultaneous Motion and Interaction Force Control of a Nonholonomic Mobile Manipulator* (Department of Mechanical and Aerospace Engineering, University at Buffalo, Buffalo, NY, 2006).